Available online at www.sciencedirect.com

ScienceDirect

Procedia CIRP 126 (2024) 975–980

www.elsevier.com/locate/procedia

17th CIRP Conference on Intelligent Computation in Manufacturing Engineering

Geometric digital twins of long-living assets: uncertainty-aware 3D images from measurement and CAD data

Keno Moenck*, Thorsten Schüppstuhl

Hamburg University of Technology, Institute of Aircraft Production Technology, Denickestraße 17, 21073 Hamburg, Germany

* Corresponding author. Tel.: +49-40-42878-3341 ; fax: +49-40-42731-4551. *E-mail address:* keno.moenck@tuhh.de

Abstract

Geometric digital twins (gDT) of long-living assets are formed from a multitude of different data sources like CAD or measurement data imaging as-designed to sensory-based acquired as-is states. Change detection techniques allow merging 3D data pairwise, deriving a geometric digital twin of the physical asset. However, positional uncertainties must be considered to account for the data's reliability when facing different kinds of data sources. The contribution of this work provides the ability to specify (an-)isotropic positional uncertainty quantities for meshes and even sparse point clouds in advance, enabling uncertainty-aware change detection. In the case of sensory-based as-is data, uncertainty is defined by the measurement process, while in the case of as-designed CAD data, the uncertainty relates, e.g., to manufacturing tolerances. Instead of testing on equal means during point-wise comparison as in M3C2, we utilize the Bhattacharyya distance measure to quantify the (dis)similarity between correspondences during change detection.

Keywords: Digital Twin; Change Detection; 3D Scanning; Measurement Uncertainty

1. Introduction

Long-living, often one-of-a-kind assets, like plants, buildings, seafaring vehicles, aircraft, or offshore oil rigs depend on value-adding and inevitable service activities, like retrofit or maintenance repair and overhaul (MRO) processes, in their different lifecycle phases to preserve their profitability [1]. An asset's digital representation – a digital twin (DT) – enables the a priori, reliable, and time-efficient planning of these activities. A DT can snapshot the asset through different states or epochs from as-designed, as-manufactured up to as-is. By epoch, we emphasize a long period between the asset changes. Initially, the as-designed or even as-is state is available as CAD data. The as-is state based on feeding information from changes or modifications back into a consistent known digital representation during the lifecycle is often inhibited, on the one hand, by information exchange barriers between the owner of the product, service providers, and suppliers, on the other hand, by non-digitized modifications and changes. Here, the market and stakeholder situation as well as the quality assurance processes, contradict the DT concept embodying data-centricity in representing the asset's physical instance in each of its epochs.

Data acquisition methods based on 3D scanning are often applied to geometrical twin the asset forming the most recent as-is state to, e.g., conduct virtual fit-checks or plan a maintenance operation. Incorporating sensory-acquired data and 3D information from previous epochs reduces the necessary amount of newly acquired data, relaxes the constrains on measurement devices uncertainty, and provides

10.1016/j.procir.2024.08.369

information on what has changed between two known states.

Merging 3D data from different epochs results in a complete 3D image of the real world, as long as objects do not change between epochs. Instead, we can use change detection techniques to separate new information from known ones. If we have an as-designed CAD model from epoch zero, only changes are imaged by lower-quality sensory-acquired data, while non-changed regions or objects remain as-designed.

The approach of merging multiple measurement and CAD data sources through change detection is subject to this work. The results after each epoch geometrical twin the asset with the most reliable information.

The rest of this paper is organized as follows: First, we present related work (Sec. 2) regarding geometric as-is state generation and discuss change detection methods. In Sec. 3, we describe the modeling of measurement uncertainties and continue in Sec. 4 with the presentation of our approach, following the experimental results in Sec. 5 and discussion and conclusion in Sec. 6.

2. Related work

Geometric digital twinning [2] comprises the idea of deriving an as-is state of an environment. After “as-designed” follows “as-build” or “as-manufactured” serving, e.g., progressive construction monitoring, while the “as-is” serves later activities in an asset’s lifecycle [3]. The methods of as-is generation based on measurement data are either point-based [4, 5] or object-based by means of the classification of components [6] or models’ parameter estimation [7]. The latter definitely requires a classification model trained on costly training data, which is for the depicted domains often not feasible. Therefore, we focus in the following on point-based, traditional methods.

Change detection refers to determining differences among a pair of records separated in time, imaging the same physical object or area. The first and probably most cited review article on this subject from 1989 [8] considered input from 2D cameras on earth-orbiting satellites. The ability to rely on more than 2D images multiplied the number of methods. Besides BIM [9] and remote sensing [10], fields like autonomous surveillance [11] or robotics [12] employ change detection techniques based on 2D/3D optical measuring systems.

We can distinguish methods of 3D change detection by their data representations, change metrics, and segmentation techniques. **Probabilistic-based** approaches abstract the reference data onto multivariate probability density functions (PDF) using, for example, cell-based Normal Distribution Transforms [11]. The assumption is that if the covariance matrix is considered as an ellipsoid, a small volume leads to a better representation of the underlying geometries, which means, e.g., two pronounced eigendirections represent a plane, a line leads to one distinct eigendirection. In contrast, [13] avoids quantization effects at the cells’ borders by estimating a Gaussian Mixture Model (GMM) using expectation maximization while increasing model size by splitting the Gaussians. Given the GMM data representation, [14] quantifies change by utilizing a spatial difference probability metric between each Gaussian. [13] estimates GMMs for both datasets and quantifies change by calculating the Earth Mover’s Distance metric between the models. In a **graph-based** approach, [15] defines tentative matches of Gaussian distributions as nodes. The matches are accepted based on graph constraints. Then, the maximum clique contains distributions that have consistent associations. Nodes having neither or one edge correspond to changes. [16] use **Boolean operations on implicit volumes** to detect changes by estimating normalized density functions, where points on the surface are mapped to zero, while points inside and outside the estimated surface map to negative and positive real values, respectively. Change extraction equals the subtraction of two implicit volumes. Probabilistic-, graph-based, and operations on implicit volumes depend on an intermediate 3D representation, also modeling the result. The traceability to the original data representation, e.g., meshes, is only feasible under the loss of information.

A different set of approaches use homologous **grid or voxel maps** representing the data as geometric primitives [17], Truncated Signed Distance Functions [18], or reflection probabilities [19]. The accumulation of points in voxels and subsequent change extraction are either used in real-time applications or on large data sets containing millions of points. Thereby, single local anomalies are not necessarily of interest. However, a finer gradation makes voxels obsolete. Besides, the sensor model must explicitly be known for reflection or occupancy maps, which is contradictory given CAD data.

The most common and straightforward methods for comparing 3D data are Cloud-to-Cloud (C2C), C2C with local modeling, Cloud-to-Mesh, and Mesh-to-Mesh distance computations. If employing point-to-point comparisons, e.g., C2C computation without local modeling, the main problem is that measurement data from two different epochs do not obey the same point sampling on real-world objects. Therefore, local modeling is necessary, as in the Multiscale-Model-to-Model-Cloud Comparison (M3C2) [20] method that explicitly considers surface roughness and noise. Winiwarter et al. [21] employ a statistical significance test to improve the M3C2 incorporating Gaussian per-point uncertainty. We will follow the idea of point-wise change detection but will not constrain the approach to points and normally distributed uncertainties.

3. (An-)isotropic positional uncertainty

A complete measurement result consists of the expectation value and an uncertainty quantity that “reflects the lack of exact knowledge of the value of the measurand,” as stated by the Guide to the Expression of Uncertainty in Measurement (GUM) [22]. A covariance matrix models the uncertainty of a multivariate measurement as in the 3D case. The uncertainties of optical 3D measuring systems are often higher in one direction due to the physical measuring principles and, e.g., the angle of the sampled surface with respect to the sensor.

Therefore, covariance matrices vary per point. We distinguish between solely estimated and sample-based uncertainties.

For the former, as in the case of the *Artec Eva* (s. Fig. 1), we propose to use the calibration results based on the point-to-mesh distance of a known scanned environment. Here, normally distributed quantities can be assumed. Contrary, according to the GUM [22], error limits modeled by isotropic piece-wise constant probability densities must be assumed if the uncertainty's underlying distribution is unknown. For example, if we do not know an object's manufacturing process but know it complies with the as-designed tolerances.

Fig. 1: 3D optical scanning systems used in the experimental evaluation (left: structured light scanner *Artec Eva*, right: low-cost ToF camera in mobile device *Lenovo Phab 2 Pro*).

3D capturing devices like low-cost handheld Time-of-Flight (ToF) cameras produce dense and noisy point clouds through their sensor characteristic and localization errors. Then, each point is an individual indication, and estimating the expectation values of points lying on the objects' surfaces is necessary. We use voxel-based Maximum Likelihood Estimation (MLE): fitting points into an overlapping voxel grid and estimating the parameters of a Multivariate Normal distribution (MVN) per voxel. Fig. 2 depicts the result of evaluating all estimated PDFs on a plane in the test scene's epoch $\boldsymbol{E_1}$ (see Sec. 6). The contour of the original underlying real-world object is guessable by following the brighter parts.

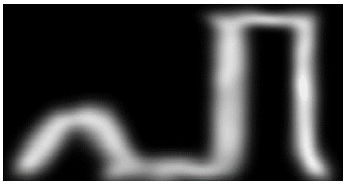

Fig. 2: Probability density functions evaluated on a plane from the test scene (s. Sec. 5.1; brighter, denser parts represent higher probabilities).

4. Change detection under uncertainty

The approach of deriving a 3D real-world image is depicted in Fig. 3, consisting of co-registration and change detection. Epoch zero ($\boldsymbol{E_0}$) consist of "as-designed" data, while all subsequent epochs ($\boldsymbol{E_x}$) consists of new measurement data imaging the "as-is" state at the moment of acquisition. Co-registration and change detection form a new composite 3D image, a snapshot of the epoch. This work does not consider the different ways of aligning point clouds and meshes through co-registration. In the experimental section, we used the Generalized-ICP [23].

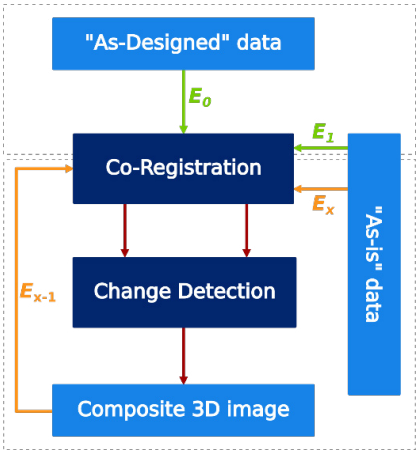

Fig. 3: The proposed concept to derive the geometric digital twin (gDT) from multiple epochs.

4.1. Region of View

The recognition of vanished objects in scenes is only viable if and only if the measured and non-measured space is known. We propose to name the measured space of a scene Region of View (ROV). Unlike real-valued discrete occupancy maps [24], the ROV provides a universal piece-wise continuous representation. We can automatically generate the ROV based on the scans' metadata, i.e., sensor model and viewpoints. In any case, the ROV has to have a closed two-dimensional manifold characteristic; it is well-defined if points or objects lie inside, outside, or on the ROV. To determine the ROV, we can apply a two-step process, where at first, a bounding box is formed based on the sensor models. The second step involves the extraction of occluded areas. We propose a straightforward technique to remove occluded areas by introducing the Plane of Sight (POS). The POS is a polygon that most likely represents a scene's different viewpoints. Then, for each reference dataset's point within the bounding box, a ray to the closest point on the POS is constructed. If that ray intersects the recent dataset an uneven number of times, the point is not enclosed in the ROV, even in the case of non-watertight meshes or multiple non-connected components. If the recent dataset consists only of a point cloud, augmenting it using a surface reconstruction algorithm to obtain an intermediate surface representation is necessary, but the constraint on the water-tightness is relaxed.

4.2. Change Computation

4.2.1. Distance measure

Given two univariate measurements, each measurement's underlying population includes all possible output readings theoretically observable with the specific measuring device and process. The population is the set of all possible indications. López et al. [25] test if one of the measuring devices obtains a higher precision to compare two point clouds. In contrast, the question can be raised whether the expectation values $\overline{\boldsymbol{x_1}}$ and $\overline{\boldsymbol{x_2}}$ differ at certain confidence by testing on equal means as utilized in the M3C2 procedure. Welch's t-test [26] expresses

how an observed value relates to an expected in terms of standard deviations. If the means do not significantly differ, the object's dimension may have changed, or one can conclude that the measurands are from different objects. In both cases, change is indicated. As an example, in Fig. 4, it is evident that the expectation value of measurement $\boldsymbol{A}$ obtained with a device of poor precision is closest to $\boldsymbol{B_1}$ in terms of the Euclidean distance. Although, based on the uncertainties, the measurements probably depict different points on an object. The device that outputs $\boldsymbol{B_2}$, on the other hand, pointed perhaps at the same position. Regarding change detection, the measurement $\boldsymbol{B_1}$ provides new information, while $\boldsymbol{B_2}$ primarily extends existing.

So, we derive two problems concerning change detection. On the one hand, we must find corresponding measurement points in the recent and reference datasets, and on the other hand, we must define a test or change metric for the multivariate case, especially having non-normally distributed quantities.

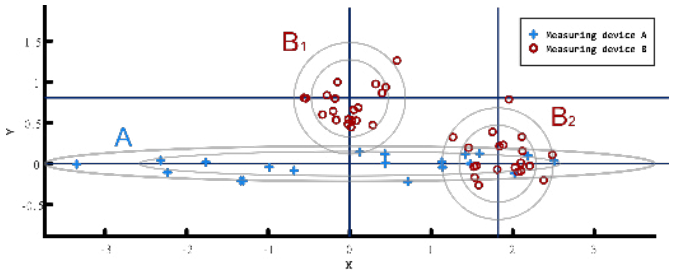

Fig. 4: Measurements from two different measuring devices possessing different uncertainties.

In a multivariate case, Hotelling's T-square test statistic replaces Welch's two-sample t-test. However, the test statistic is only proved in the case of MVNs. For non-normally distributed quantities, a non-parametric simulation-based test would have to be used to reject the null hypothesis on equal means per correspondence. This is way too computationally expensive, which leads us to propose using the Bhattacharyya Distance (BD) to quantify the dissimilarity between two corresponding points. Based on that, we apply a "change"/"no change" mask. The BD and Bhattacharyya coefficient (BC) (Eq. 7,3 [27]) are defined as:

$$BC = \int \sqrt{p_1(\boldsymbol{x}) \cdot p_2(\boldsymbol{x})}\, d\boldsymbol{x}\,,$$

$$BD = -\ln(BC)\,,$$

where p_1 and p_2 represent PDFs. The BC ranges in [0; 1], while the upper bound depicts $p_1 = p_2$. To explain the BD, given two normal distributions with mean $\boldsymbol{\mu_i}$ and covariance matrices $\boldsymbol{\Sigma_i}$, the divergence forms as follows (Eq. 3 [28]):

$$BD\langle \mathcal{N}(\boldsymbol{\mu_1}, \boldsymbol{\Sigma_1}), \mathcal{N}(\boldsymbol{\mu_2}, \boldsymbol{\Sigma_2})\rangle = \frac{1}{8}(\boldsymbol{\mu_2} - \boldsymbol{\mu_1})^T \boldsymbol{\Sigma}^{-1}(\boldsymbol{\mu_2} - \boldsymbol{\mu_1}) + \frac{1}{2}\ln\left[\frac{\det \boldsymbol{\Sigma}}{\sqrt{\det \boldsymbol{\Sigma_1}\ \det \boldsymbol{\Sigma_2}}}\right],$$

where the matrix $\boldsymbol{\Sigma}$ depicts the mean of $\boldsymbol{\Sigma_1}$ and $\boldsymbol{\Sigma_2}$. The first term is related to the Mahalanobis distance, while the second term expresses the differences between the distributions' (co-) variances. If $\boldsymbol{\Sigma_1} = \boldsymbol{\Sigma_2}$ the second term vanishes, and the BD is proportional to the squared Mahalanobis distance, informally stating how many standard deviations the means are apart.

The BD can not be used for statistical significance testing since it does not obey a consistent asymptotically distribution. As a result, we can not state a critical value to apply a binary change mask. The BD generally depends very much on the size of the uncertainties' error ellipsoids. Therefore, we propose using as an initial value of each change detection iteration a multiple of the sensitivity, the error tolerance ε_T during numerical integration. If a more reliable statement is desired, the change threshold τ can be derived by a simulation-based two-sample t-test indicating a significant change through testing on equal means.

4.2.2. Correspondence estimation

In the proposed concept, facets of a mesh are treated as an agglomeration of infinite points so that it is enough to specify the uncertainty parameters for each one or all facets combined. This approach allows us to oppose points and facets without defining a function that continuously maps a facet's probability density in space.

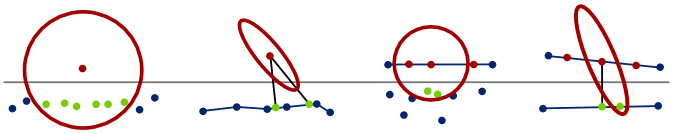

Fig. 5: Estimating correspondences (increased distance between datasets for illustration; red: search space and query points, blue dots: point cloud, blue lines: facets, green: estimated correspondences, black: search rays).

We obtain four different cases where we have to estimate correspondences (s. Fig. 5). In the point-to-point case, the nearest neighbors within a 99% probability sphere transferred into a mixture model are used for each query point. If a query point faces a mesh, the first intersection point is determined based on the most distinct uncertainty direction and the closest point in terms of Euclidean distance to account for isotropic uncertainty. In the mesh-to-point case, we propose to sample random points on a facet and utilize the same procedure as for the point-to-point case. In the mesh-to-mesh case, random points are sampled on each facet; then, the point-to-mesh procedure is applied. The lowest change quantity is accepted for the whole facet in both cases.

5. Experimental results

5.1. Test scene

To illustrate the concept, we created a fictitious test scene consisting of three different geometric primitives (s. Fig. 6): two different-sized cuboids, and two frustums of the same dimensions. The scene's datasets consist of manually modeled CAD data ($\boldsymbol{E_0}$) and measurements obtained with the two measuring systems mentioned in Sec. 3. Four different epochs were arranged. For simplicity, we manually created the bounding boxes and the POSs to determine the ROVs. The

bottom row in Fig. 6 depicts the resulting as-is states after registration and change detection. In $\boldsymbol{E_1}$, we introduced the larger cuboid into the scene. The as-is dataset is noisy and of less precision. However, our method can extract the changes; points sampled on the cuboid are segmented as depicted in the composite 3D image ***a)*** (Fig. 6). $\boldsymbol{E_2}$ was acquired with the *Artec Eva*. Since its ROV encloses the ROV of $\boldsymbol{E_1}$, as of $\boldsymbol{E_2}$, the previously known measurement data are replaced by the newly acquired with higher precision. Finally, $\boldsymbol{E_3}$ images only parts of the scene, where two objects were removed. For illustration purposes, we blended in the removed objects' wireframes (marked in red).

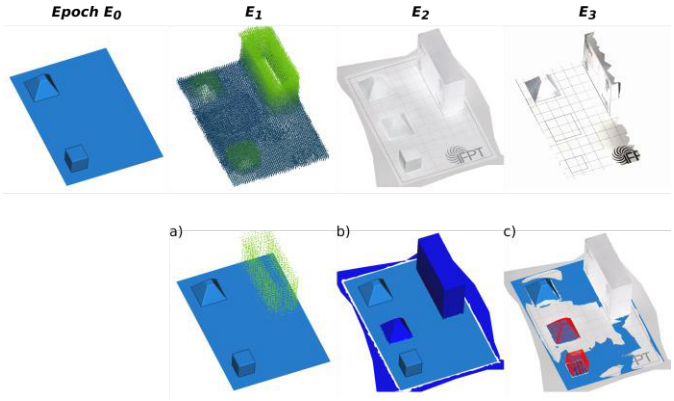

Fig. 6: Top row: the test scene's four consecutive epochs $\boldsymbol{E_x}$. Bottom row: the resulting composite 3D image after each epoch.

5.2. Aircraft fuselage and structural components

An aircraft's lifecycle exceeds its interior by a significant factor, as airlines regularly convert an aircraft's cabin to meet the current needs of passengers or VIP customers. Acquiring a complete 3D image of the aircraft cabin and fuselage is a task for a Design Organization planning the modification [29]. The cabin is attached to the fuselage structure through brackets and fittings. To validate our approach, we created two epochs (s. Fig. 7), where we introduced and removed brackets in $\boldsymbol{E_1}$.

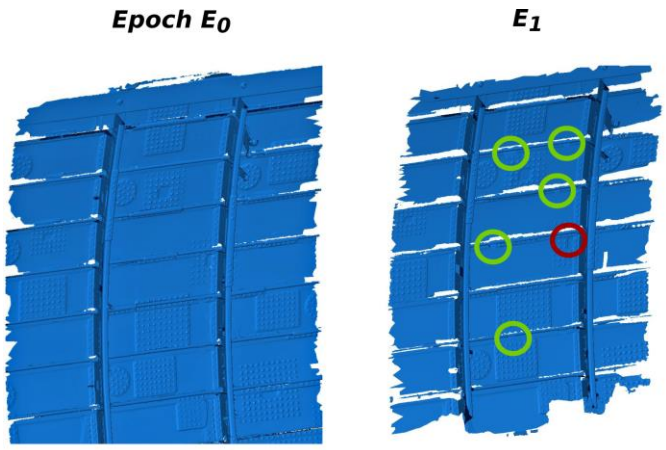

Fig. 7: Two different epochs of an aircraft fuselage section acquired with the *Artec Eva*. We added five and removed one bracket in $\boldsymbol{E_1}$.

A section of the result after the change detection is shown in Fig. 8. A newly added bracket is segmented in the result. However, it appears to float because of the resulting gap between the stringer and the bracket's front side. On the one hand, this results from *Artec Eva*'s measurement uncertainty and mesh resolution; on the other hand, the chosen change threshold τ does not allow for finer gradation on the boundaries. Nevertheless, the result is sufficient for the actual engineering application, cabin retrofitting, since the geometric center of the bracket can be accurately obtained.

As expected, all facets representing parts of $\boldsymbol{E_1}$ that do not provide any new information, like the fuselage's stringer, frames, and skin are from the previous epoch. However, one measurement artifact was recognized as a novelty (see ***a)*** in Fig. 8).

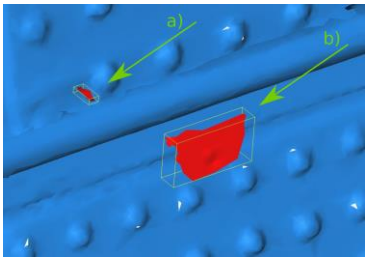

Fig. 8: Section from the composite 3D image after $\boldsymbol{E_1}$ (***b)*** is showing a newly observed bracket).

6. Discussion and conclusion

The epoch-by-epoch creation and updating of a 3D image forming a geometric DT are subject to different domains around long-living assets. In contrast to other related works, we addressed supporting various data sources whose outputs have different levels of precision. We are the first to explicitly include the support of non-normally distributed uncertainties, as required by the Guide to the Expression of Uncertainty (GUM), as soon as the information basis on quantities is not sufficient. Besides, we presented a practical and straightforward method to determine the space captured by an optical 3D measuring system, the ROV. It is required to detect vanished objects in only partly overlapping scans. By continuously modeling the ROV based on the sensor model and viewpoints, we do not have to rely on discrete maps and achieve a much higher resolution. We experimentally evaluated the concept using a generic scene and demonstrated it in an aircraft cabin retrofitting context.

Future work may include the semantic enrichment of the epochs supported by the change detection results.

Acknowledgments

This work is part of the research project *Intelligent Digital Cabin Twin (InDiCaT)*, supported by the *Federal Ministry for Economic Affairs and Climate Action* as part of the *Federal Aeronautical Research Programme LuFo VI-1*.

Supported by:
Federal Ministry for Economic Affairs and Climate Action
on the basis of a decision by the German Bundestag

References

[1] Moenck, K., Laukotka, F., Krause, D., Schüppstuhl, T., 2022. Digital Twins of existing long-living assets: reverse instantiation of the mid-life twin, in *DS 119: Proceedings of the 33rd Symposium Design for X (DFX2022)*.

[2] Lu, Q., Chen, L., Li, S., Pitt, M., 2020. Semi-automatic geometric digital twinning for existing buildings based on images and CAD drawings *115*, p. 103183.

[3] Lu, Q., Lee, S., 2017. Image-Based Technologies for Constructing As-Is Building Information Models for Existing Buildings *31*, p. 4017005.

[4] Tran, H., Khoshelham, K., 2019. Building change detection through comparison of a lidar scan with a building information model *XLII-2/W13*, p. 889.

[5] Anil, E.B., Tang, P., Akinci, B., Huber, D., 2013. Deviation analysis method for the assessment of the quality of the as-is Building Information Models generated from point cloud data *35*, p. 507.

[6] Wang, C., Cho, Y.K., Kim, C., 2015. Automatic BIM component extraction from point clouds of existing buildings for sustainability applications *56*, p. 1.

[7] Cheng, Y.-J., Qiu, W.-G., Duan, D.-Y., 2019. Automatic creation of as-is building information model from single-track railway tunnel point clouds *106*, p. 102911.

[8] Singh, A., 1989. Review Article Digital change detection techniques using remotely-sensed data *10*, p. 989.

[9] Previtali, M., Barazzetti, L., Brumana, R., Scaioni, M., 2014. Towards automatic indoor reconstruction of cluttered building rooms from point clouds *II-5*, p. 281.

[10] Awrangjeb, M., 2015. Effective Generation and Update of a Building Map Database Through Automatic Building Change Detection from LiDAR Point Cloud Data *7*, p. 14119.

[11] Andreasson, H., Magnusson, M., Lilienthal, A., 2007. Has something changed here? Autonomous difference detection for security patrol robots, in *2007 IEEE/RSJ International Conference on Intelligent Robots and Systems*, IEEE, p. 3429.

[12] Manso, L.J., Núñez, P., Silva, S.d., Drews-Jr, P., 2014. A Novel Robust Scene Change Detection Algorithm for Autonomous Robots Using Mixtures of Gaussians *11*, p. 18.

[13] Nunez, P., Drews, P., Rocha, R., Campos, M. *et al.*, 2009 - 2009. Novelty detection and 3D shape retrieval based on Gaussian Mixture Models for autonomous surveillance robotics, in *2009 IEEE/RSJ International Conference on Intelligent Robots and Systems*, IEEE, p. 4724.

[14] Silva Filho, S., Drews-Jr, P., Botelho, S., 2014. Detecting Changes in 3D Maps using Gaussian distribution.

[15] P. Nunez, P. Drews, A. Bandera, R. Rocha, M. Campos, J. Dias, 2010 - 2010. Change detection in 3D environments based on Gaussian Mixture Model and robust structural matching for autonomous robotic applications, in *2010 IEEE/RSJ International Conference on Intelligent Robots and Systems*, IEEE, p. 2633.

[16] Vieira, A.W., Drews, P.L.J., Campos, M.F.M., 2012. *Efficient change detection in 3D environment for autonomous surveillance robots based on implicit volume*. Institute of Electrical and Electronics Engineers (IEEE).

[17] Katsura, U., Matsumoto, K., Kawamura, A., Ishigami, T. *et al.*, 2019. Spatial change detection using voxel classification by normal distributions transform, in *2019 International Conference on Robotics and Automation (ICRA)*, IEEE, [Piscataway, NJ], p. 2953.

[18] Fehr, M., Furrer, F., Dryanovski, I., Sturm, J. *et al.*, 2017 - 2017. TSDF-based change detection for consistent long-term dense reconstruction and dynamic object discovery, in *2017 IEEE International Conference on Robotics and Automation (ICRA)*, IEEE, p. 5237.

[19] Luft, L., Schaefer, A., Schubert, T., Burgard, W., 2018. Detecting Changes in the Environment Based on Full Posterior Distributions Over Real-Valued Grid Maps *3*, p. 1299.

[20] Lague, D., Brodu, N., Leroux, J., 2013. Accurate 3D comparison of complex topography with terrestrial laser scanner: Application to the Rangitikei canyon (N-Z) *82*, p. 10.

[21] Winiwarter, L., Anders, K., Höfle, B., 2021. M3C2-EP: Pushing the limits of 3D topographic point cloud change detection by error propagation *178*, p. 240.

[22] ISO/IEC. ISO/IEC Guide 98-3:2008(E), Uncertainty of measurement - Part 3: Guide to the expression of uncertainty in measurement (GUM:1995), Berlin. Beuth Verlag GmbH, 2008(Guide 98-3).

[23] Segal, A., Haehnel, D., Thrun, S., 2010. Generalized-ICP, in *Robotics: Science and systems V*, MIT Press, Cambridge, MA.

[24] Elfes, A., 1989. Using occupancy grids for mobile robot perception and navigation *22*, p. 46.

[25] Asís López, F. de, Ordóñez, C., Roca-Pardiñas, J., García-Cortés, S., 2014. Point cloud comparison under uncertainty. Application to beam bridge measurement with terrestrial laser scanning *51*, p. 259.

[26] Welch, B.L., 1947. The Generalization of `Student's' Problem when Several Different Population Variances are Involved *34*, p. 28.

[27] Kailath, T., 1967. The Divergence and Bhattacharyya Distance Measures in Signal Selection *15*, p. 52.

[28] Basener, W., Flynn, M., 2018. Microscene evaluation using the Bhattacharyya distance, in *Multispectral, Hyperspectral, and Ultraspectral Remote Sensing Technology, Techniques and Applications VII: 24-26 September 2018, Honolulu, Hawaii, United States*, SPIE, Bellingham, Washington, USA, p. 29.

[29] Moenck, K.H.W., Laukotka, F.N., Deneke, C., Schüppstuhl, T. *et al.*, 2022. Towards an Intelligent Digital Cabin Twin to Support an Aircraft's Retrofit and Base Maintenance, in *SAE Technical Paper Series*, USA